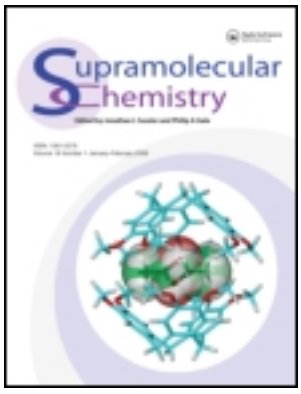

Supramolecular Chemistry
Publication details, including instructions for authors and subscription information:
http://www.tandfonline.com/loi/gsch20

Modification of MOF catalysts by manipulation of counter-ions: experimental and theoretical studies of photochemical hydrogen production from water over microporous diruthenium (II, III) coordination polymers

Yusuke Kataoka [b], Yuhei Miyazaki [a], Konomi Sato [a], Toru Saito [b], Yasuyuki Nakanishi [b], Yasutaka Kiatagwa [b], Takashi Kawakami [b], Mitsutaka Okumura [b], Kizashi Yamaguchi [b] & Wasuke Mori [a]

[a] Department of Chemistry, Faculty of Science, Kanagawa University, Hiratsuka, Japan
[b] Department of Chemistry, Graduate School of Science, Osaka University, Toyonaka, Japan

Available online: 13 Apr 2011

To cite this article: Yusuke Kataoka, Yuhei Miyazaki, Konomi Sato, Toru Saito, Yasuyuki Nakanishi, Yasutaka Kiatagwa, Takashi Kawakami, Mitsutaka Okumura, Kizashi Yamaguchi & Wasuke Mori (2011): Modification of MOF catalysts by manipulation of counter-ions: experimental and theoretical studies of photochemical hydrogen production from water over microporous diruthenium (II, III) coordination polymers, Supramolecular Chemistry, 23:03-04, 287-296

To link to this article: http://dx.doi.org/10.1080/10610278.2010.527976

Supramolecular Chemistry
Vol. 23, Nos. 3–4, March–April 2011, 287–296

Modification of MOF catalysts by manipulation of counter-ions: experimental and theoretical studies of photochemical hydrogen production from water over microporous diruthenium (II, III) coordination polymers

Yusuke Kataoka[b]*, Yuhei Miyazaki[a], Konomi Sato[a], Toru Saito[b], Yasuyuki Nakanishi[b], Yasutaka Kiatagwa[b], Takashi Kawakami[b], Mitsutaka Okumura[b], Kizashi Yamaguchi[b] and Wasuke Mori[a]*

[a]*Department of Chemistry, Faculty of Science, Kanagawa University, Hiratsuka, Japan;* [b]*Department of Chemistry, Graduate School of Science, Osaka University, Toyonaka, Japan*

(*Received 7 July 2010; final version received 19 September 2010*)

In this study we investigated the photochemical production of hydrogen from water using three heterogeneous microporous ruthenium coordination polymers $[Ru_2(p\text{-}BDC)_2X]_n$ (p-BDC = 1,4-benzenedicarboxylate, X = Cl, Br and BF_4) in the presence of multi-component systems. The order of catalytic performances is $[Ru_2(p\text{-}BDC)_2Br]_n > [Ru_2(p\text{-}BDC)_2BF_4]_n > [Ru_2(p\text{-}BDC)_2Cl]_n$. The most active catalyst, $[Ru_2(p\text{-}BDC)_2Br]_n$, caused the evolution of 46.7 μmol hydrogen molecules with a turn-over number of 18.7 based on $[Ru_2(p\text{-}BDC)_2Br]_n$ under visible light irradiation for 4 h. We ascertained that the differences in catalytic activities originated from (1) the efficiency of the quenching of methyl-viologen radicals by $[Ru_2(p\text{-}BDC)_2X]_n$ and (2) the durability of the structure in the reaction. In order to examine the catalytic reaction mechanism, we performed theoretical calculations for neutral model structures $[Ru_2(HCOO)_4X(H_2O)]$ (X = Cl, Br), one-electron reduction model complexes $[Ru_2(HCOO)_4X(H_2O)]^-$ and deduced intermediate model structures $[H{-}Ru_2(HCOO)_4X]$ using broken-symmetry hybrid density functional theory methods.

Keywords: water splitting; coordination polymers; metal organic frameworks

1. Introduction

The purification and storage of hydrogen molecules are matters of interest to researchers in the academic as well as industrial fields. For this purpose, the photochemical production of hydrogen from water using visible light is being investigated thoroughly with the aim of developing an efficient method for converting solar radiation into chemical energy. A number of active homogeneous or heterogeneous catalyst systems have been developed in the past several decades (*1–3*). Such systems, called light-harvesting systems (LHSs), usually contain a photosensitiser (PS) such as $Ru(bpy)_3^{2+}$, an electron relay (ER) such as methyl-viologen (MV^{2+}), several sacrificial donors (SDs) and a hydrogen production catalyst (HPC) such as Pt nanoclusters (Scheme 1) (*4*, *5*).

Although heterogeneous metal colloid or semiconductor HPCs have been extensively studied thus far, relatively fewer studies have been conducted on complex HPCs (*6*). However, complex HPCs have been shown to exhibit catalytic activity and can be obtained by cost-effective and environmentally friendly routes. Moreover, the use of complex HPCs is indispensable in fields such as photochemistry and processes such as artificial photosynthesis. Therefore, these HPCs are still in the developmental stage and several aspects of this relatively new technology are yet to be explored.

In recent years, several important studies have been conducted on the photochemical or electrical production of hydrogen from water using complex HPCs. For example, Sakai et al. (*7*) performed studies on the reduction of water into molecular hydrogen by electrochemically generated MV^+ molecules in the presence of mononuclear or dinuclear platinum complexes, without requiring an external PS or SD. In other words, their studies demonstrated that the molecular sources of hydrogen were the aqueous protons or hydronium ions in the reaction solution, and that hydrogen was not produced by the decomposition of an SD. Bernhard et al. (*8*) reported the photochemical production of D_2 from the D_2O/acetonitrile/triethanolamine media using an $[Ir(ppy)_2(bpy)]^+$ PS and a platinum catalyst. This result also indicated that the generation of hydrogen was mainly on account of the aqueous protons and not the decomposition of the SD. The groups of Gray and Dubois (*9*, *10*) have pointed out the importance of the thermodynamics of H binding to the active site for the hydrogen evolution reaction by a complex HPC. Several theoretical studies have been conducted to clarify the catalytic reaction mechanisms of photochemical hydrogen production from

*Corresponding authors. Email: kataoka@chem.sci.osaka-u.ac.jp; wmori@kanagawa-u.ac.jp

ISSN 1061-0278 print/ISSN 1029-0478 online

DOI: 10.1080/10610278.2010.527976
http://www.informaworld.com

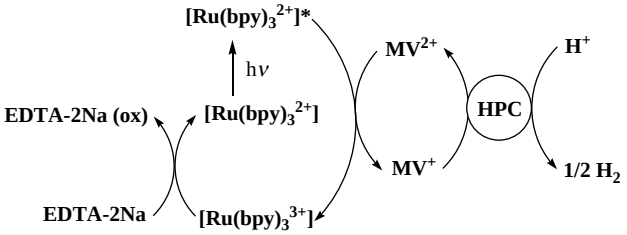

Scheme 1. LHS for photochemical hydrogen production.

water by a complex HPC. For example, to provide some insight into the stability of a Pt(II)-Cl analogous complex HPC, Batista et al. (*11*) reported the density functional theory (DFT) and TD-DFT calculations for $Pt(H_2$-dcbpy)Cl_2 and found that while this compound was stable after reduction, the photoexcitation of the reduced species led to the dissociation of the ligand set. In other words, they postulated that the colloidal Pt was the source of H_2 produced in the experiments by a Pt–Cl analogous complex HPC. These theoretical results agreed with the experimental facts reported by Eisenberg and Hammarstrom (*12*, *13*). Recently, Hall, Gioia and Koper (*14–16*) have independently reported the DFT-calculated interaction energies for the bonding between H and a hydrogenase model structure. These calculations are important for enabling the development of complex HPCs, because they aid in evaluating the intermediate complex, which is otherwise difficult to evaluate by experimental studies.

Microporous coordination polymers called metal-organic frameworks (MOFs) consisting of metal ions and organic ligands with highly regularised cavities or channels are an emerging class of porous materials. This structural feature inspired many chemists to further investigate such polymers for their potential zeolite-like applications, mostly in fields such as gas-occlusion properties (*17–19*). At present, their applications are focused not only on the determination of gas adsorption properties but also on improving heterogeneous catalytic performance. From the perspective of heterogeneous catalysis, we categorised MOF catalysts into two groups. One group consists of those used for the deposition of a metal colloid on MOFs (*20*). The other group consists of 'self-supported catalysts' that function as heterogeneous catalysts without other activity sites such as metal colloid or semiconductor (*21*). Thus far, we have demonstrated the catalytic reaction of self-supported catalysts using a variety of copper, rhodium and ruthenium coordination polymers with poly-carboxylic acids (*22–27*). As an example, we have recently demonstrated that $[Ru_2(p$-$BDC)_2BF_4]_n$ (p-BDC = 1.4-benzendicarboxylate) caused H_2 gas evolution from an aqueous solution in the presence of a multi-component system containing $Ru(bpy)_3^{2+}$, MV^{2+} and ethylenediaminetetraacetato-2Na (EDTA-2Na) under visible-light illumination (*28*). $Ru_2(CH_3$-$COO)_4BF_4$, which formed a similar building-block structure, was also used as a homogeneous complex HPC in the same reaction solution ($Ru(bpy)_3^{2+}$, MV^{2+} and EDTA-2Na). However, the catalytic activity of $Ru_2(CH_3$-$COO)_4BF_4$ was evidently lower than that of $[Ru_2(p$-$BDC)_2BF_4]_n$. The same tendency was also observed between heterogeneous catalyst $[Rh_2(p$-$BDC)_2]_n$ or $[Zn\{Pd(INA)_4\}]_n$ (INA = Isonicotinate) and homogeneous catalyst $Rh_2(C_6H_5COO)_4$ or $Pd(H\text{-}INA)_2(INA)_2$, respectively (*29*, *30*). Therefore, it is advantageous to use coordination polymers in HPC materials. We found that the reason for the observed high catalytic performance was the effective electron transfer (ET) caused by the physical adsorption of the ER (MV^{2+}) occurring on the surface of the coordination polymers.

As a next step, in order to develop the MOF HPC, we studied the surface modification of the MOF HPC because hydrogen production reaction almost occurred on the surface of MOF HPC. As the easily modification, we paid attention to counter-ions of building blocks of MOF. In this paper, we describe the photochemical production of hydrogen from water using three microporous ruthenium coordination polymers $[Ru_2(p\text{-}BDC)_2X]_n$ (X = Cl; Ru—Cl, X = Br; Ru—Br and X = BF_4; Ru—BF_4) in the presence of $Ru(bpy)_3^{2+}$, MV^{2+} and EDTA-2Na. Moreover, we also discuss the studied gas-adsorption properties, MV^{2+} adsorption, photochemical MV^+ generation, catalyst stability and theoretical calculations.

2. Experimental

2.1 Materials

All reagents and solvents were purchased from commercial sources and were used without further purification. $[Ru_2(CH_3COO)_4X]_n$ and $[Ru_2(p\text{-}BDC)_2X]_n$ were synthesised using methods described in the literature (*31–33*).

2.2 Measurement procedure

$[Ru_2(p\text{-}BDC)_2X]_n$ powders were observed by SEM (FE-SEM S-4000, Hitachi Co., Tokyo, Japan). FT-IR spectra were recorded on a JASCO 4100 FT-IR spectrometer on a KBr disc at room temperature in the 800–2000 cm^{-1} region. XPS measurements were recorded on JPS-9010 (JEOL) with a Mg Kα X-ray source (10 kV, 10 mA). The UV–vis spectra were measured on a JASCO V-660 spectrophotometer.

N_2 gas adsorption measurements at 77 K were carried out using an ASAP2010 volumetric adsorption analyser (Shimadzu Co., Kyoto, Japan). A sample was dried overnight before its treatment under high vacuum at 300 K and for 3 h at 393 K to remove the solvated water. During the measurements and before the treatment,

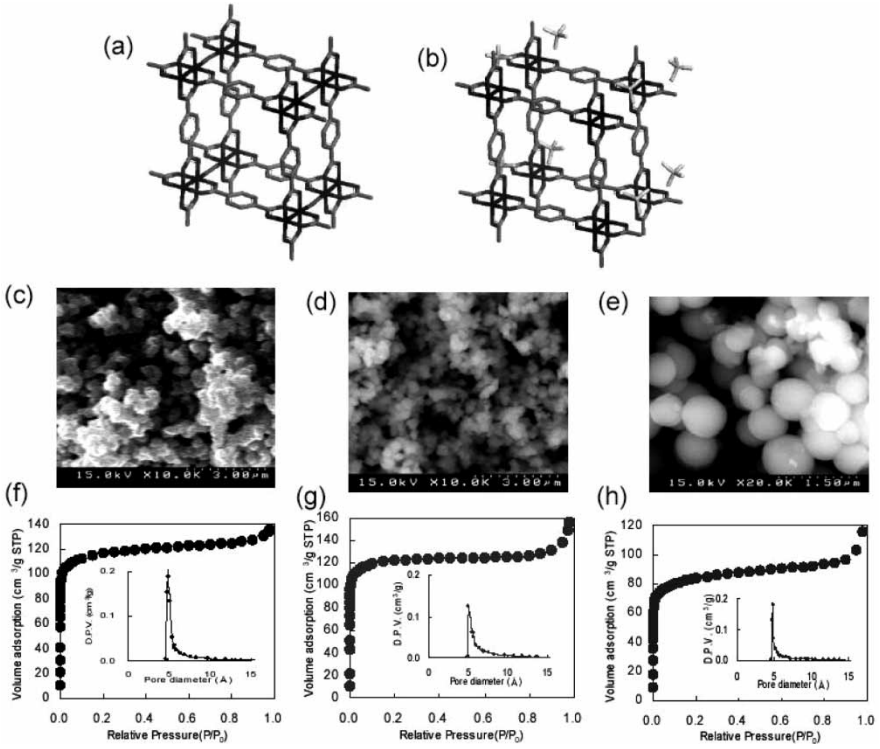

Figure 1. Self-assembly coordination structures of (a) Ru—X (X = Cl, Br) and (b) Ru—BF_4, SEM image (c: Ru—Cl, d: Ru—Br, e: Ru—BF_4) and adsorption isotherms (f: Ru—Cl, g: Ru—Br, h: Ru—BF_4, pore diameter distributions were inserted in each graphs, DPV = differential pore volume).

we used ultra-high-purity grades (99.9999%) of N_2 (for gas analysis) and He (for gas analysis in free space).

2.3 Photocatalytic reaction method

All photocatalytic reactions were performed in a closed gas circulation system with a Pyrex reaction cell. The typical reaction solution (10 ml) containing EDTA-2Na (150 mM), $Ru(bpy)_3Cl_2$ (0.1 mM) and MV^{2+}(5.0 mM) was degassed by repeated freeze-pump-thaw cycles. Before treatment, synthesised HPC was ground with agate mortar (see, SEM images; Figure 1). Next, the reaction solution and ground HPC (0.005 mmol) were shifted into the reaction vessel with a glovebox under an Ar-saturated atmosphere. The reaction solution was irradiated at 300 K using a 500 W Xe lamp (USHIO Co., Tokyo, Japan) equipped with an optical cut-off filter ($\lambda > 420$ nm). The amount of evolved H_2 was determined using a gas chromatograph (Shimadzu; GC-14B, with TCD and FID detectors, a stainless-steel column packed with molecular sieves-5A, and ultra-pure Ar carrier gas). All measurements were performed under non-oxygen conditions. The quantum yield (QY), defined by the equation given below, was measured using a combined band-pass and cut-off (Kenko, Tokyo, Japan) filter (450 nm irradiation) and a photodiode (PM3; Coherent).

$$\mathrm{QY} = \frac{(\text{number of reacted electrons})}{(\text{number of incident photons})} \times 100$$

$$= \frac{(\text{number of evolved } H_2 \text{ molecules} \times 2)}{(\text{number of incident photons})} \times 100,$$

where the number of incident photons is 8.81×10^{-5}.

2.4 MV^{2+} adsorption measurement

To confirm whether MV^{2+} was adsorbed on $[Ru_2(p\text{-}BDC)_2X]_n$ in aqueous media, we measured the amount of MV^{2+} molecules in the UV–vis spectrum. An adsorption solution (10 ml) containing 0.02 mmol $[Ru_2(p\text{-}BDC)_2X]_n$ and 0.1 mM MV^{2+} was stirred for 1 h.

2.5 Photochemical MV^{+} generation

The time taken for the generation of MV^{+} radical ions was measured using a JASCO V-660 spectrophotometer and 500 W Xe lamp equipped with a band-pass and a cut-off filter (450 nm irradiation). The reaction solution containing 0.005 mol HPC and LHS solution (10 ml; 0.1 mM $Ru(bpy)_3^{2+}$, 5.0 mM MV^{2+} and 150.0 mM EDTA-2Na)

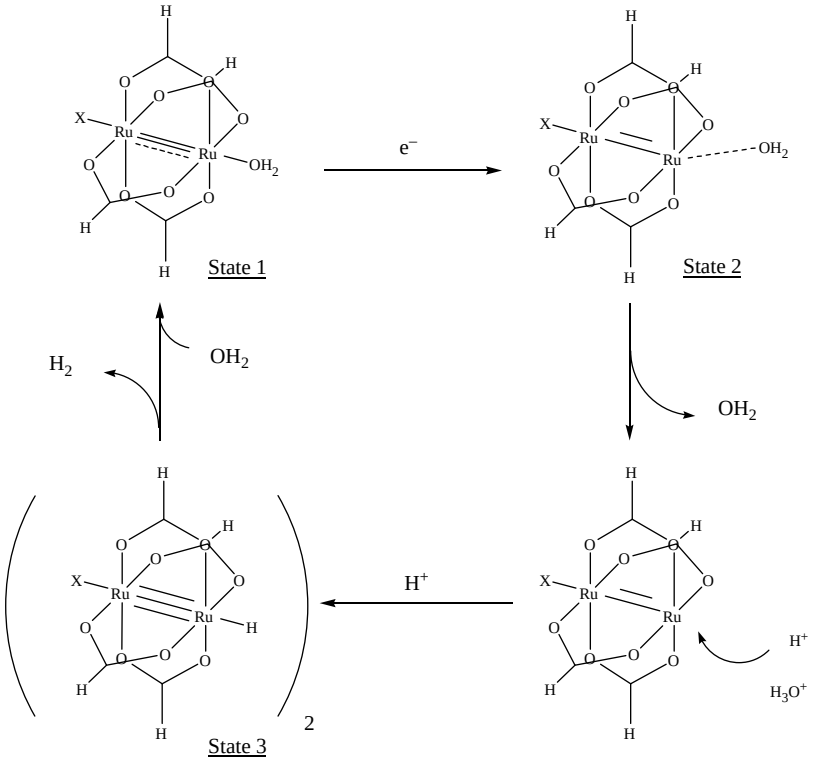

Scheme 2. Model structures for theoretical calculations and deduced catalytic mechanism (X = Cl and Br).

was irradiated. All measurements were performed under non-oxygen conditions.

2.6 Computational procedure for theoretical calculations

All quantum chemical calculations were performed using the LANL2DZ basis set for Ru atoms; the 6-31G** basis set for H, C and O atoms; and the 6-311G** for halogen atoms. A spin-unrestricted, i.e. broken symmetry (BS), method was employed for the open-shell calculation; UB3LYP was used with Gaussian 09 program packages (*34*). We performed calculations for neutral model structures $[Ru_2(HCOO)_4X(H_2O)]$ (State 1, X = Cl, Br), one-electron reduction structures $[Ru_2(HCOO)_4X(H_2O)]^-$ and deduced intermediate model structures [H—$Ru_2(HCOO)_4X$] (State 3) considering them as model structures. For the one-electron reduction structures, we performed calculations using two geometries. One used was neutral model geometry (State 1′), the other was optimised geometry of $[Ru_2(HCOO)_4X(H_2O)]^-$ (State 2). These model structures and deduced catalytic mechanisms are shown in Scheme 2. All the geometries were fully optimised without any constraints of symmetry. Furthermore, the optimised structures were characterised using harmonic frequency calculations.

3. Results and discussion

3.1 Materials

The self-assembled molecular structures, SEM images and nitrogen adsorption isotherms of $[Ru_2(p\text{-BDC})_2X]_n$ are shown in Figure 1. Particle sizes measured from SEM images and adsorption parameters (Langmuir and BET surface areas, pore volume and pore diameter) are listed in Table 1.

Table 1. Adsorption parameters and particle size of $[Ru_2(p\text{-BDC})_2X]_n$.

	Surface area (m^2/g)				
	Langmuir	BET	Pore diameter (Å)	Pore volume (cm^3/g)	Particle size (μm)
Ru—Cl	525.5	345.6	4.9	0.18	<1.0
Ru—Br	543.8	379.3	5.0	0.19	<0.5
Ru—BF_4	413.8	288.4	4.8	0.14	<1.2

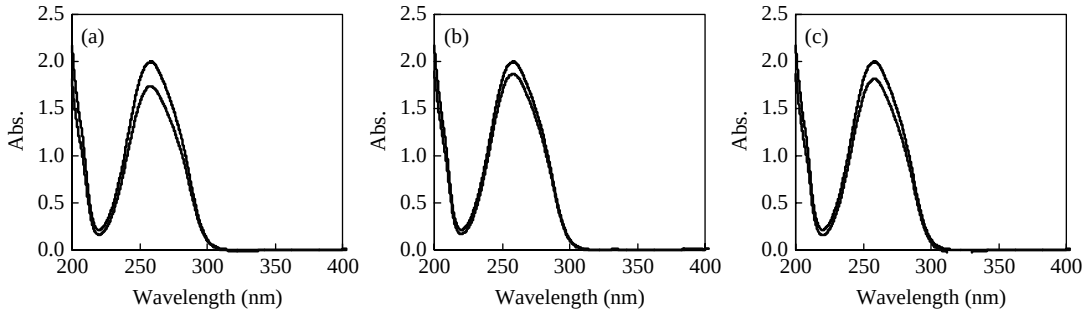

Figure 2. MV^{2+}-adsorption on $[Ru_2(p\text{-}BDC)_2X]_n$ in H_2O media. (a: Ru—Cl, b: Ru—Br, c: Ru—BF_4, upside: 0 h, down side: 1 h).

In terms of structural geometries, Ru—Cl and Ru—Br complexes have a 3D jungle-gym-like structure, in which a 2D square grid sheet composed of a dinuclear ruthenium (II, III) paddle-wheel motif with a *p*-BDC organic linker is bridged by halogen counter-ions to extend the 2D structure to a 3D structure (Figure 1(a)). Therefore, this material formed an -M-M-X- mixed-valence structure and the 2.5 oxidation state of the ruthenium atoms. On the other hand, the structure of Ru—BF_4 did not form a 3D structure. The 2D slit sheets of Ru—BF_4 were stacked without interpenetration, and the BF_4 counter-ions were located in the coordination spaces. (Figure 1(b)).

From Figure 1(c)–(e), we can observe that the SEM images of Ru—BF_4 have almost spherical particles approximately 1.2 μm in diameter, whereas those of Ru—Cl and Ru—Br have polyhedral shapes that are less than 0.5 and 1.0 μm in diameter.

In order to determine the microporous capacity of these materials, we measured the nitrogen gas adsorption isotherm of a sample of dehydrated $[Ru_2(p\text{-}BDC)_2X]_n$ at 77.4 K. The nitrogen isotherm of the $[Ru_2(p\text{-}BDC)_2X]_n$ showed a sharp nitrogen uptake at low pressures; this uptake is called micropore filling. Micropore filling can be classified as an IUPAC type-I behaviour. Although the trend of the nitrogen adsorption isotherm of Ru—Cl was similar to that of Ru—Br, the isotherm of Ru—BF_4 was obviously low because BF_4 counter-ions were located in those cavities. The specific surface area (Langmuir, BET), maximum amount of N_2 adsorbed, pore diameter Horvath–Kawazoe method and pore volume Dubinin–Radushkevich method are listed in Table 1. The pore diameter was almost equal for all three complexes; however, only Ru—BF_4 had a low pore volume for existence of BF_4 counter-ions in its cavities. The Langmuir surface areas for Ru—Cl, Ru—Br and Ru—BF_4 were 525.5, 543.8 and 413.8 m^2/g, respectively. These results seem to indicate that the MV^{2+} molecules ($6.3 \times 6.3 \times 13.4$ Å) were not adsorbed into the cavities of these HPCs (4.8–5.0 Å).

3.2 MV^{2+} adsorption on HPCs

In order to confirm whether MV^{2+} was adsorbed into the pores or on the surface of $[Ru_2(p\text{-}BDC)_2X]_n$ in aqueous media, we measured the UV–vis spectrum. Figure 2(a)–(c) shows the time taken for the MV^{2+} adsorption on Ru—Cl, Ru—Br and Ru—BF_4, respectively.

These results show a small decrease in the absorption band of MV^{2+} (258 nm). The decrease in the amount of MV^{2+} molecules in Ru—Cl, Ru—Br and Ru—BF_4 are 12.9, 6.2 and 9.1%, respectively. From the minute difference in the amount of MV^{2+} molecules adsorbed on these three catalysts, we ascertained that the MV^{2+} molecules could not be adsorbed on the cavities of $[Ru_2(p\text{-}BDC)_2X]_n$, and the MV^{2+} molecules were adsorbed on the surface of an $[Ru_2(p\text{-}BDC)_2X]_n$. The same phenomenon, i.e. MV^{2+} adsorption on the surface of HPC, has also been reported for semiconductor particles, Pt catalysts and coordination polymers (*35*, *36*).

3.3 Photocatalytic reaction

The photochemical reduction of water using $[Ru_2(p\text{-}BDC)_2X]_n$ was performed in the presence of $Ru(bpy)_3^{2+}$, MV^{2+} and EDTA-2Na. The time taken for H_2 evolution is shown in Figure 3.

The initial slopes of H_2 evolution for Ru—Cl, Ru—Br and Ru—BF_4 were measured to be 5.55, 15.2 and 7.33 μmol, respectively. Prolonged irradiation led to an increase in H_2 production. The amount of evolved H_2 and the turn-over number (TON) after 4 h of irradiation are listed in Table 2. From Table 2, it can be noted that the amount of H_2 evolved after 4 h of irradiation was in the following order: $[Ru_2(p\text{-}BDC)_2Br]_n$ (46.7 μmol) > $[Ru_2(p\text{-}BDC)_2BF_4]_n$ (23.5 μmol) > $[Ru_2(p\text{-}BDC)_2Cl]_n$ (13.5 μmol). The TON of the most active catalyst, Ru—Br, was 18.7 and that of $Ru(bpy)_3^{2+}$ was 93.4. Although the catalytic performance in this case was lower than that of $[Ru_2(p\text{-}BDC)_2X]_n$, the reaction systems using the diruthenium acetate complexes, i.e. $Ru_2(CH_3COO)_4X$ (X = Cl, Br and BF_4), were also observed to induce

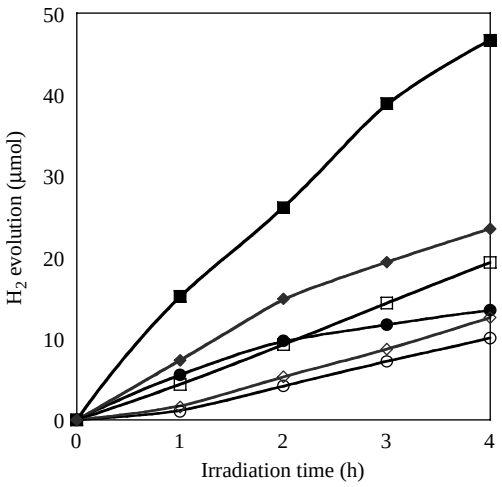

Figure 3. Time course of He evolution from 10 ml aqueous solution consisting of 0.1 mM $Ru(bpy)_3^{2+}$, 5.0 mM MV^{2+}, 150 mM EDTA-2Na and 0.005 mmol HPCs (■: Ru—Br, ◆: Ru—BF_4, ●: Ru—Cl, □: $Ru_2(CH_3COO)_4Br$, ◇: $Ru_2(CH_3COO)_4BF_4$, ○: $Ru_2(CH_3COO)_4Cl$).

H_2 production in the same LHS solutions ($Ru(bpy)_3^{2+}$, MV^{2+} and EDTA-2Na). Interestingly, the order of catalytic performance after the 4 h irradiation was [$Ru_2(CH_3COO)_4Br$] (19.7 μmol) > [$Ru_2(CH_3COO)_4BF_4$] (12.6 μmol) > [$Ru_2(CH_3COO)_4Cl$] (10.0 μmol); this order is the same as that observed for $[Ru_2(p\text{-}BDC)_2X]_n$. Therefore, the difference in the catalytic performance of $[Ru_2(p\text{-}BDC)_2X]_n$ was obviously a result of the surface modification, which could be attributed to the selection of the counter-ions. This is because the measured adsorption parameters and particle sizes of $[Ru_2(p\text{-}BDC)_2X]_n$ were not substantially different from those of $[Ru_2(CH_3COO)_4X]_n$. The results of control experiments indicated that all the components, namely, $[Ru_2(p\text{-}BDC)_2X]_n$, $Ru(bpy)_3^{2+}$, MV^{2+} and EDTA-2Na, were essential for H_2 evolution; the absence of any one of them produced anywhere from unobservable to insignificant amounts of H_2 gas. As expected, no H_2 evolution was detected in the dark. Under the same light-harvesting conditions, the activity of Ru—Br was 16.5 and 1.37 times greater than those of anatase-TiO_2 (BET surface area: 40.0 m^2/g, 2.83 μmol H_2 at 4 h) and $Pt(bpy)Cl_2$ (34.2 μmol H_2 at 4 h), respectively.

3.4 *Time course of photochemical MV^+ generation*

Next, we studied the photoreduction of MV^{2+} to MV^+ in a typical reaction solution under 450 nm light irradiation and its accompanying ET from MV^+ to $[Ru_2(p\text{-}BDC)_2]_n$. For this, we measured the time-dependent UV–vis spectra. (See Figure 4; the strong 450 nm band is assigned to the metal to ligand charge transfer band of $Ru(bpy)_3^{2+}$.)

As shown in Figure 4(a), non-$[Ru_2(p\text{-}BDC)_2X]_n$ conditions were evidently generated for MV^+ because the reaction solution exhibits two strong absorption bands at 392 and 603 nm that can be attributed to the transition of the MV^+ radical. On the other hand, in Figure 4(b)–(d), increases in the width of these absorption bands were also observed when $[Ru_2(p\text{-}BDC)_2X]_n$ was present, but the amount of absorption in these cases was much lower. This phenomenon suggested that the MV^+ radicals were quenched by $[Ru_2(p\text{-}BDC)_2X]_n$. The amount of the generation of MV^+ at 1 h was measured to be in the following order: $[Ru_2(p\text{-}BDC)_2Cl]_n$ (Abs.: 1.13 at 603 nm) > $[Ru_2(p\text{-}BDC)_2BF_4]_n$ (Abs.: 1.01 at 603 nm) > $[Ru_2(p\text{-}BDC)_2Br]_n$ (Abs.: 0.950 at 603 nm). While prolonged irradiation led to increased MV^+ molecules in the systems employing Ru—Cl (Abs.: 1.28 at 603 nm at 4 h) and Ru—BF_4 (Abs.: 1.26 at 603 nm at 4 h), the MV^+ molecules in the system that employed Ru—Br (Abs.: 1.02 at 603 nm at 4 h) did not vary similarly. It is interesting to note that the time taken for H_2 evolution and MV^+ generation is related and that the most active catalyst, $[Ru_2(p\text{-}BDC)_2Br]_n$, was observed to generate the least number of MV^+ molecules. That is, these results strongly demonstrate that efficient ET occurred from MV^+ to $[Ru_2(p\text{-}BDC)_2X]_n$ and that the ET efficiency was directly related to the catalytic reaction activity.

3.5 *Theoretical calculations*

In order to investigate the catalytic reaction mechanism and compare the most active Br analogue complex with the least active Cl analogue complex, we performed BS-DFT calculations of neutral model complexes (State 1),

Table 2. H_2 evolution and TON at 4 h irradiation and quantum efficiency (ϕ) of catalytic reaction.

HPC	H_2 production (μmol)	TON-based HPC	TON-based $Ru(bpy)_3^{2+}$	ϕ (%)
Ru—Cl	13.5	5.38	26.9	0.711
Ru—Br	46.7	18.7	93.4	3.75
Ru—BF_4	23.5	9.4	47.0	2.36
$Ru_2(CH_3COO)_4Cl$	10.0	4.02	20.1	–
$Ru_2(CH_3COO)_4Br$	19.7	7.75	38.7	–
$Ru_2(CH_3COO)_4BF_4$	12.6	5.04	25.2	–

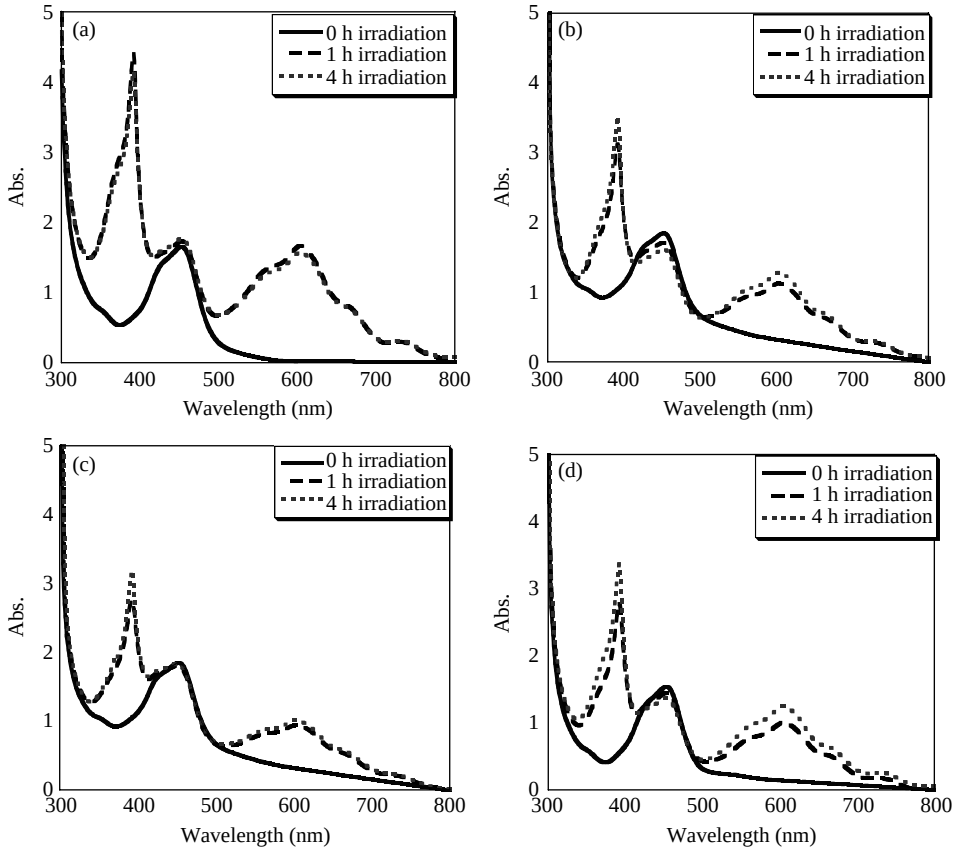

Figure 4. Time course of MV^+ generation (at 0, 1 and 4 h) in the presence of $Ru(bpy)_3^{2+}$, MV^{2+}, EDTA-2Na and HPCs. (a) non-catalyst, (b) Ru—Cl, (c) Ru—Br and (d) Ru—BF_4.

one-electron reduction model complexes (State 1′ and State 2) and intermediate model complexes (State 3). Optimised geometrical parameters for the same are listed in Table 3.

In neutral complexes (State 1), the electronic configurations of both counter-ions became $\pi^2\delta^2\sigma^2\delta*\pi*^2$. The optimised Ru—Ru lengths for the Cl and Br analogues were 2.365 and 2.370 Å, respectively. The Cl and Br counter-ions formed a bonding orbital with the $Ru_2(d\pi)$ and $Ru_2(d\pi*)$ orbitals, and the binding energies for Ru—X, i.e. E_{bind}(Ru—X), were 121.4 and 121.5 kcal/mol for Ru—Cl and Ru—Br, respectively. On the other hand, the OH_2 molecules interacted with the $Ru_2(d\sigma)$ orbital. The binding energies for Ru—OH_2, i.e. E_{bind}(Ru—OH_2), were 13.73 (Cl analogue) and 13.71 kcal/mol (Br analogue). Therefore, in State 1, no obvious gap was observed between Cl and Br counter-ions.

In the one-electron reduction model, the electrons occupied the Ru_2 ($d\delta*$) orbital. In this scenario, electron affinities ($= E_{total}$(state 1′) $- E_{total}$(state 1)) were calculated to be 64.8 and 64.4 kcal/mol. These differences were negligible in the case of the small gap and could not explain the difference between the catalytic activities. Geometrical optimisation of the one-electron reduction model, $[Ru_2(HCOO)_4X(H_2O)]^-$ (State 2), showed the relaxation of the Ru—Ru bond and ligands surrounding the Ru from neutral complexes. It is interesting to note that since H_2O molecules were dissociated from the Ru_2 axial

Table 3. Geometrical parameters (Å) of optimised geometries of model structures.

	Ru–Ru	Ru—X	Ru—O(Ac)	Ru—O(H_2)	Ru—H
$[Ru_2(OOCH)_4Cl(H_2O)]$	2.365	2.406	2.048–2.087	2.498	–
$[Ru_2(OOCH)_4Br(H_2O)]$	2.370	2.555	2.050–2.088	2.488	–
$[Ru_2(OOCH)_4Cl(H_2O)]^-$	2.342	2.495	2.097–2.123	3.034	–
$[Ru_2(OOCH)_4Br(H_2O)]^-$	2.343	2.652	2.097–2.123	2.998	–
[H—$Ru_2(OOCH)_4Cl$]	2.644	2.385	2.069–2.084	–	1.560
[H—$Ru_2(OOCH)_4Br$]	2.648	2.516	2.069–2.087	–	1.559

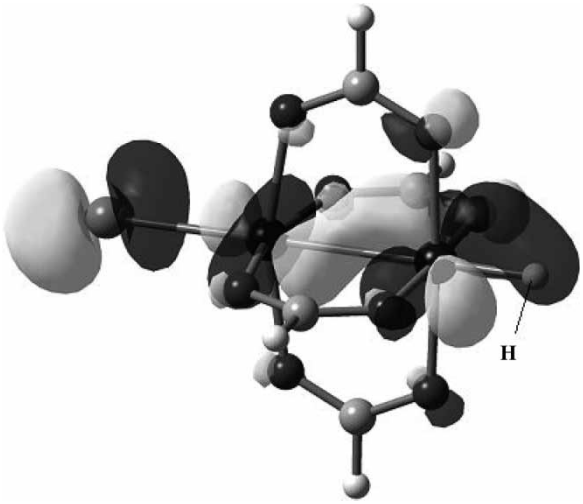

Figure 5. Highest single occupied molecular orbital (H-SOMO) of optimised structure of intermediated model complex [H—Ru_2(HCOO)$_4$Br].

site by Coulomb repulsion interaction, the open metal site appeared in the Ru_2 axial site. On the other hand, increases in the Ru—Cl and Ru—Br lengths were within 0.1 Å, and their E_{bind}(Ru—X) values reduced to 37.08 and 37.07 kcal/mol, respectively.

In intermediate model complexes (State 3), we confirmed that lengths of the optimised structures of the Ru–Ru and Ru—Cl were greater than those in State 2. The comparison between the Mulliken electronic charges of the Ru_2 unit of State 2 (Cl analogue: 0.96, Br analogue: 0.87) and that of State 3 (Cl analogue: 1.32, Br analogue:1.21) suggested that charge transfer occurred from the Ru_2 to the H atom. As shown in Figure 5, the H atom formed a bonding orbital with $Ru_2(d\pi*)$. The binding energies, i.e. E_{bind}(Ru—H), are 35.5 (Cl analogue) and 36.3 kcal/mol (Br analogue). These results indicate that the difference in the values of the affinity of the Ru—H bond could not be confirmed.

As mentioned above, the theoretical calculations performed in this study indicate that the potential catalytic activities between Ru—Cl and Ru—Br complexes were almost equal. Therefore, the origin of differential catalytic activities of $[Ru_2(p\text{-BDC})_2X]_n$ were speculated for other processes such as counter-exchange and structural decomposition.

3.6 Stability of HPCs

Finally, in order to prove the stability of the catalysts in this reaction, the catalysts were characterised before and after the reaction by measuring the XPS and FT-IR spectra. These spectra are shown in Figures 6 and 7.

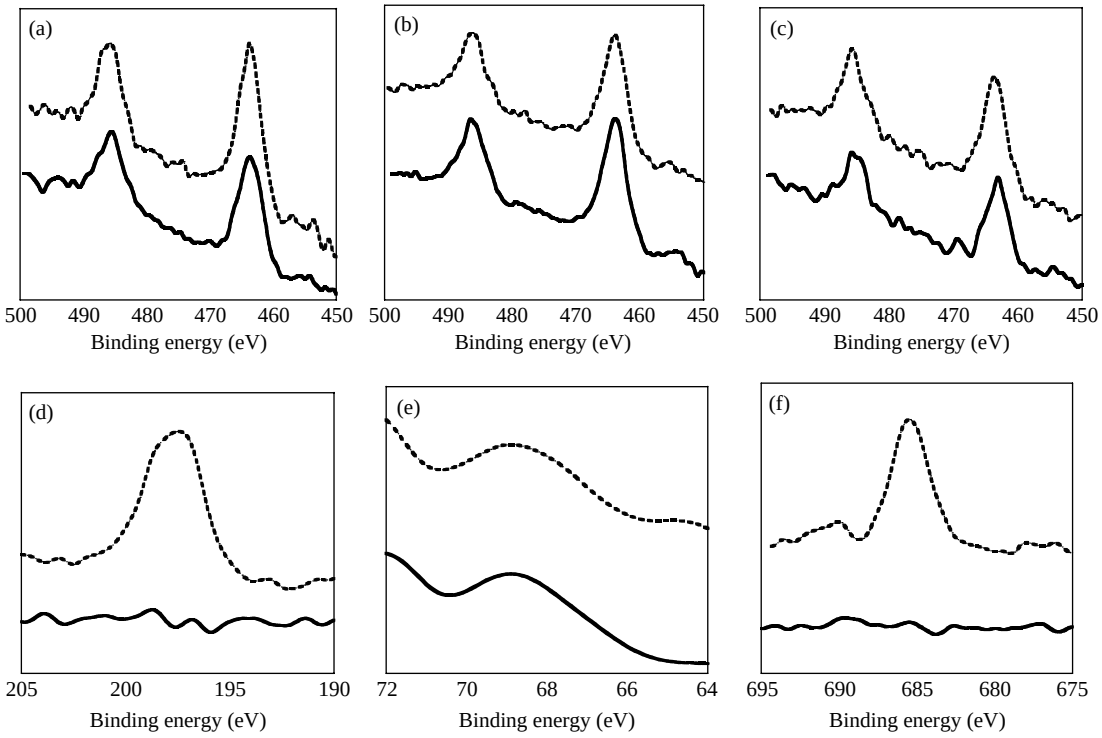

Figure 6. XPS spectra of $[Ru_2(p\text{-BDC})_2X]_n$ before and after catalytic reaction (dash line: before reaction, solid line: after reaction). Ru3p doublet ($3p_{3/2}$ and $3p_{1/2}$) of (a) Ru—Cl, (b) Ru—Br and (c) Ru—BF_4. (d) Cl 2p peak of Ru—Cl. (e) Br $3d_{5/2}$ peak of Ru—Br. and (f) F 1S peak of Ru—BF_4.

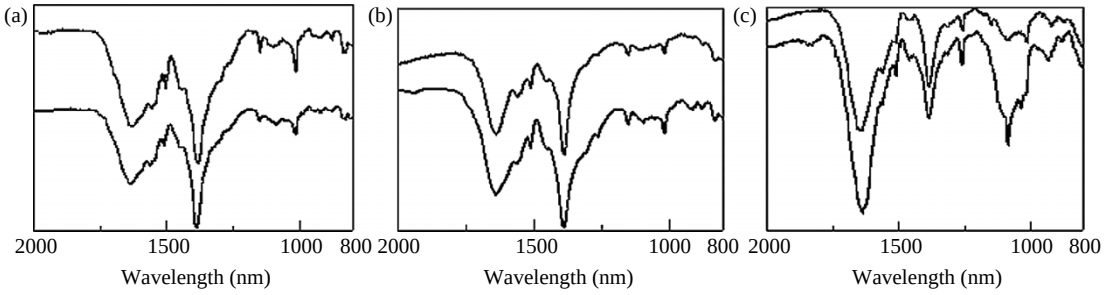

Figure 7. FT-IR spectra of $[Ru_2(p\text{-}BDC)_2X]_n$ before and after catalytic reaction (down side: before reaction, upside: after reaction). (a) Ru—Cl, (b) Ru—Br and (c) Ru—BF_4.

In the XPS spectrum, the Ru^{II}-Ru^{III} 3p doublet ($3p_{3/2}$ and $3p_{1/2}$) of the three HPCs before and after the catalytic reaction appeared at normal Ru_2^{5+} values of around 463 and 485 eV, respectively, without any obvious gap. No new binding energies were observed. From these data, it was confirmed that the valency of Ru does not change. In other words, these results prove that photo-colloidalisation of $[Ru_2(p\text{-}BDC)_2X]_n$ did not occur. However, while Br $3d_{5/2}$ peaks in Ru—Br were found at around 68.8 eV after the reaction, Cl 2p in Ru—Cl and F $1s_{1/2}$ peaks in Ru—BF_4 disappeared after the reaction. We speculated that the Cl and BF_4 counter-ions were substituted with EDTA or the oxidation products of EDTA during the process of the catalytic reaction. In fact, the result of an elemental analysis revealed that a small quantity of Cl counter-ions converted into EDTA ions on stirring the solution containing 150 mM EDTA solution and 10.0 mg Ru—Cl complex (before stirring: N 0.0% → after 4 h stirring: N 1.0%), even non-light irradiation. As the EDTA ions could not enter the pores of $[Ru_2(p\text{-}BDC)_2X]_n$, we supposed that the counter-ion exchange only occurred near the surface of $[Ru_2(p\text{-}BDC)_2X]_n$.

In the FT-IR spectrum of $[Ru_2(p\text{-}BDC)_2X]_n$, the main peaks formed due to the vibrations of the organic linker before and after the catalytic reactions did not change. In the spectra of Ru—BF_4, only a BF_4 vibration peak (at 1083 cm^{-1}) disappeared; however, other vibration peaks remained unchanged. These positive results demonstrated that the frameworks of $[Ru_2(p\text{-}BDC)_2X]_n$ were stable in this catalytic reaction. In other words, photocatalytic activities are characteristic properties of $[Ru_2(p\text{-}BDC)_2X]_n$. From these experimental studies, we can say that the decrease in the catalytic performance originated from the counter-ion exchange near the surface of $[Ru_2(p\text{-}BDC)_2X]_n$ and not the decomposition of the frameworks of $[Ru_2(p\text{-}BDC)_2X]_n$.

4. Conclusion

We successfully demonstrated the modification of an MOF catalyst by the manipulation of counter-ions. While theoretically calculated results such as electron affinities and binding energies did not differ substantially between Ru—Cl and Ru—Br, the order of observed catalytic activity was as follows: Ru—Br > Ru—BF_4 > Ru—Cl. The most active catalyst, $[Ru_2(p\text{-}BDC)_2Br]_n$, showed the highest catalytic activity with 46.7 μmol H_2 evolution and a TON of 18.7. These values were superior to the well-researched values obtained for a Pt molecular catalyst, $Pt(bpy)Cl_2$ and anatase-TiO_2. Characterisations of the samples after the catalytic reaction showed that the Cl and BF_4 counter-ions disappeared and were substituted with EDTA, and that only the Ru—Br catalyst maintained the coordination geometry between Ru and Br counter-ions. Subsequently, the Ru—Br catalyst did not lose its potential catalytic activity and exhibited effective catalytic performance. From these results, we could confirm that the catalytic activity of MOF with counter-ions altered noticeably when the counter-ions were manipulated by molecular catalyst, and the design of MOF catalysts required an adequate examination of counter-ions for the purpose of reaction. Our group is currently conducting related studies on MOF catalysts with counter-ions and on other catalytic reactions.

Acknowledgements

One of the authors (Y. Kataoka) expresses his special thanks to the Global center of excellence (COE) Program 'Global Education and Research Center for Bio-Environmental Chemistry' of Osaka University. This work was supported by a Grant-in-Aid for Specially Promoted Research (No. 19350077) from the Ministry of Education, Culture, Sports, Science and Technology of Japan.

References

(1) Borgarello, E.; Kiwi, J.; Pelizzetti, E.; Viska, M.; Gratzel, M. *J. Am. Chem. Soc.* **1981**, *103*, 6324–6329.
(2) Fukuzumi, S. *Eur. J. Inorg. Chem.* **2008**, *9*, 1351–1362.
(3) Sakai, K.; Ozawa, H. *Coord. Chem. Rev.* **2007**, *251*, 2753–2766.
(4) Kalyanasundaram, K.; Kiwi, J.; Gratzel, M. *Helv. Chim. Acta* **1978**, *61*, 2720–2730.

(5) Okura, I.; Kim-Thuan, N. *J. Mol. Catal.* **1979**, *5*, 311–314.
(6) Esswein, A.J.; Nocera, D.G. *Chem. Rev.* **2007**, *107*, 4022–4047.
(7) Yamauchi, K.; Masaoka, S.; Sakai, K. *J. Am. Chem. Soc.* **2009**, *131*, 8404–8406.
(8) Tinker, L.L.; Mcdaniel, N.D.; Curtin, P.N.; Smith, C.K.; Ireland, M.J.; Bernhard, S. *Chem. Eur. J.* **2007**, *13*, 8726–8732.
(9) Dempsey, J.L.; Brunschwig, B.; Winkler, J.R.; Gray, H.B. *Acc. Chem. Res.* **2009**, *42*, 1995–2004.
(10) Dubois, M.R.; Dubois, D.L. *Acc. Chem. Res.* **2009**, *42*, 1974–1982.
(11) Roy, L.E.; Scalmani, G.; Kobayashi, R.; Batista, E.R. *Dalton Trans.* **2009**, *34*, 6719–6721.
(12) Du, P.; Schneider, J.; Li, F.; Zhao, W.; Patel, U.; Castellano, F.N.; Eisenberg, R. *J. Am. Chem. Soc.* **2008**, *130*, 5056–5058.
(13) Lei, P.; Hedlund, M.; Lomoth, R.; Rensmo, H.; Johansson, O.; Hammarstrom, L. *J. Am. Chem. Soc.* **2008**, *130*, 26–27.
(14) Surawatanawong, P.; Hall, M.B. *Inorg. Chem.* **2010**, *49*, 5737–5747.
(15) Greco, C.; Zampella, G.; Bertini, L.; Bruschi, M.; Fantucci, P.; Gioia, L.D. *Inorg. Chem.* **2007**, *46*, 108–116.
(16) Koper, M.T.M.; Bouwman, E. *Angew. Chem. Int. Ed.* **2010**, *49*, 3723–3725.
(17) Mori, W.; Inoue, F.; Yoshida, K.; Nakayama, H.; Takamizawa, S.; Kishita, M. *Chem. Lett.* **1997**, *26*, 1219–1220.
(18) Li, H.; Eddaoudi, M.; O'Keeffe, M.; Yaghi, O.M. *Nature* **1999**, *402*, 276–279.
(19) Takamizawa, S.; Nakata, E.; Yokoyama, H.; Mochizuki, K.; Mori, W. *Angew. Chem. Int. Ed.* **2003**, *42*, 4331–4334.
(20) Ishida, T.; Nagaoka, M.; Akita, T.; Haruta, M. *Chem. Eur. J.* **2008**, *14*, 8456–8460.
(21) Wang, Z.; Chen, G.; Ding, K. *Chem. Rev.* **2009**, *109*, 322–359.
(22) Kato, C.N.; Hasegawa, M.; Sato, T.; Yoshizawa, T.; Inoue, T.; Mori, W. *J. Catal.* **2005**, *230*, 226–236.
(23) Naito, S.; Tanibe, E.; Saito, T.; Miyao, T.; Mori, W. *Chem. Lett.* **2001**, *11*, 1178–1179.
(24) Sato, T.; Mori, W.; Kato, C.N.; Yanaoka, E.; Kuribayashi, T.; Ohtera, R.; Shiraishi, Y. *J. Catal.* **2005**, *232*, 186–198.
(25) Ohmura, T.; Mori, W.; Hiraga, H.; Ono, M.; Nishimoto, Y. *Chem. Lett.* **2002**, *32*, 468–469.
(26) Kato, C.N.; Ono, M.; Hino, T.; Ohmura, T.; Mori, W. *Catal. Commun.* **2006**, *7*, 673–677.
(27) Kato, C.N.; Mori, W. *C.R. Chimica* **2007**, *10*, 284–294.
(28) Kataoka, Y.; Sato, K.; Miyazaki, Y.; Masuda, K.; Tanaka, H.; Naito, S.; Mori, W. *Energy Environ. Sci.* **2009**, *2*, 397–400.
(29) Kataoka, Y.; Sato, K.; Miyazaki, Y.; Suzuki, Y.; Tanaka, H.; Kitagawa, Y.; Kawakami, T.; Okumura, M.; Mori, W. *Chem. Lett.* **2010**, *39*, 358–359.
(30) Miyazaki, Y.; Kataoka, Y.; Kitagawa, Y.; Okumura, M.; Mori, W. *Chem. Lett.* **2010**, *39*, 878–880.
(31) Takamizawa, S.; Yamaguchi, K.; Mori, W. *Inorg. Chem. Commun.* **1998**, *1*, 177–178.
(32) Takamizawa, S.; Ohmura, T.; Yamaguchi, K.; Mori, W. *Mol. Cryst. Liq. Cryst.* **2000**, *342*, 199–204.
(33) Castro, M.A.; Roitberg, A.E.; Cukiernik, F.D. *Inorg. Chem.* **2008**, *47*, 4682–4690.
(34) Frisch, M.J.; Trucks, G.W.; Schlegel, H.B.; Scuseria, G.E.; Robb, M.A.; Cheeseman, J.R.; Scalmani, G.; Barone, V.; Mennucci, B.; Petersson, G.A.; Nakatsuji, H.; Caricato, M.; Li, X.; Hratchian, H.P.; Izmaylov, A.F.; Bloino, J.; Zheng, G.; Sonnenberg, J.L.; Hada, M.; Ehara, M.; Toyota, K.; Fukuda, R.; Hasegawa, J.; Ishida, M.; Nakajima, T.; Honda, Y.; Kitao, O.; Nakai, H.; Vreven, T.; Montgomery, J.A., Jr.; Peralta, J.E.; Ogliaro, F.; Bearpark, M.; Heyd, J.J.; Brothers, E.; Kudin, K.N.; Staroverov, V.N.; Kobayashi, R.; Normand, J.; Raghavachari, K.; Rendell, A.; Burant, J.C.; Iyengar, S.S.; Tomasi, J.; Cossi, M.; Rega, N.; Millam, N.J.; Klene, M.; Knox, J.E.; Cross, J.B.; Bakken, V.; Adamo, C.; Jaramillo, J.; Gomperts, R.; Stratmann, R.E.; Yazyev, O.; Austin, A.J.; Cammi, R.; Pomelli, C.; Ochterski, J.W.; Martin, R.L.; Morokuma, K.; Zakrzewski, V.G.; Voth, G.A.; Salvador, P.; Dannenberg, J.J.; Dapprich, S.; Daniels, A.D.; Farkas, Ö.; Foresman, J.B.; Ortiz, J.V.; Cioslowski, J.; Fox, D.J. *Gaussian 09*; Revision A.1, Gaussian, Inc.: Wallingford CT, 2009.
(35) Kleijn, J.M.; Rouwendal, E.; Leeuwen, H.P.V.; Lyklema, J. *J. Photochem. Photobiol. A-Chem.* **1988**, *44*, 29–50.
(36) Beden, B.; Enea, O.; Hahn, F.; Lamy, C. *J. Electroanal. Chem.* **1984**, *170*, 357–361.